

# Materials Discovery with Extreme Properties via AI-Driven Combinatorial Chemistry

Hyunseung Kim<sup>1†</sup>, Haeyeon Choi<sup>2,3†</sup>, Dongju Kang<sup>1†</sup>, Won  
Bo Lee<sup>1\*</sup> and Jonggeol Na<sup>2,3\*</sup>

<sup>1</sup>School of Chemical and Biological Engineering, Seoul National  
University, Gwanak-ro 1, Gwanak-gu, Seoul, 08826, Republic of  
Korea.

<sup>2</sup>Department of Chemical Engineering and Materials Science,  
Ewha Womans University, 52, Ewhayeodae-gil, Seodaemun-gu,  
Seoul, 03760, Republic of Korea.

<sup>3</sup>Graduate Program in System Health Science and Engineering,  
Ewha Womans University, 52, Ewhayeodae-gil, Seodaemun-gu,  
Seoul, 03760, Republic of Korea.

\*Corresponding author(s). E-mail(s): [wblee@snu.ac.kr](mailto:wblee@snu.ac.kr);  
[jgna@ewha.ac.kr](mailto:jgna@ewha.ac.kr);

<sup>†</sup>These authors contributed equally to this work.

## Abstract

The goal of most materials discovery is to discover materials that are superior to those currently known. Fundamentally, this is close to extrapolation, which is a weak point for most machine learning models that learn the probability distribution of data. Herein, we develop AI-driven combinatorial chemistry, which is a rule-based inverse molecular designer that does not rely on data. Since our model has the potential to generate all possible molecular structures that can be obtained from combinations of molecular fragments, unknown materials with superior properties can be discovered. We theoretically and empirically demonstrate that our model is more suitable for discovering better materials than probability distribution-learning models. In an experiment aimed at discovering molecules that hit seven target properties, our model discovered 1,315 of all target-hitting molecules and 7,629 of five target-hitting molecules out of 100,000 trials, whereas the probability distribution-learning models failed. To illustrate the performance in actual problems,

we also demonstrate that our models work well on two practical applications: discovering protein docking materials and HIV inhibitors.

**Keywords:** Materials discovery, Materials extrapolation, Out-of-distribution, AI-driven combinatorial chemistry, Fragment-based RL

## 1 Introduction

The task of discovering materials that are superior to those currently known is a challenging problem in various fields of materials science, including pharmaceutical materials[1–4], electrical and electronic materials[5–11], energy materials[11–14], metals and ceramics[10], nanomaterials[15], and polymeric materials[16, 17]. Some of these studies aim to discover materials with two or more target properties that contradict each other, meaning it is difficult for them to coexist[18]. For example, super engineering plastics used in automobiles should be lighter than metals yet have similar mechanical strength[16, 17]. Similarly, transparent conductors used in display panels should be both optically transparent (requiring a large bandgap) and electrically conductive (requiring high carrier concentration, which generally has a low bandgap)[5, 18]. In some cases, the aim is to discover materials that have properties with either extremely high or low values. For example, the development of a better organic light-emitting diode (OLED) requires chemists to discover novel materials with higher efficiency and stability[6–8]. Here, the problem is that there are no (or few) known samples that have such properties compared to common materials. This makes it difficult for chemists to gain insights or knowledge from the known materials, that could help to infer the molecular structures of the desired materials. Unfortunately, this situation also holds for most machine learning models that learn the data. Therefore, it is necessary to develop a model that can discover materials, even in regions with little or no known data. In this paper, we refer to this problem as *materials extrapolation*.

In recent years, it has been reported that machine learning techniques can solve many challenging problems in a wide range of fields, including materials discovery. In particular, models for goal-directed inverse molecular design are attractive because they can directly infer the molecular structures that meet a set of given target conditions such as scaffolds[2, 19], physical properties[15, 20–22], and biological activities[2, 4, 22]. Some of these studies have proposed models based on neural machine translation (NMT) such as seq2seq[22, 23] and Transformer[24], which translate input target conditions to corresponding molecular structures. Models based on conditional generative models have also been proposed, such as conditional generative adversarial networks (cGANs)[25] and conditional variational autoencoders (cVAEs)[26]. These models directly generate molecular structures to meet a set of given target conditions[15, 19–21]. In contrast, there are also ways to obtain the

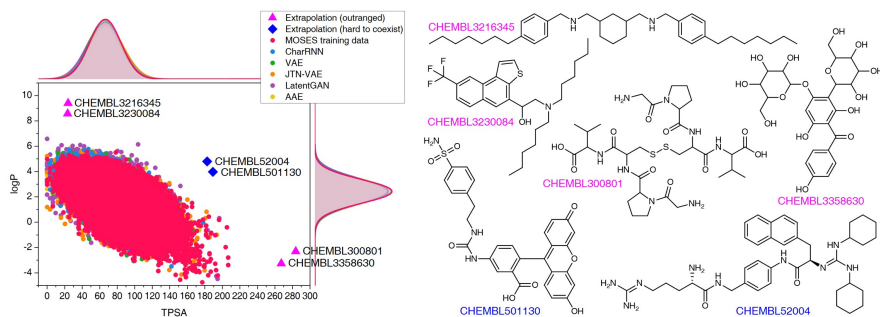


**Fig. 1 Comparison of molecular data distribution.** The red dots in the left-hand side figure denote the molecules in MOSES[33] training data. The other dots denote the molecules generated by MOSES baseline models which were trained with MOSES training data. Since the MOSES baseline models are probability distribution-learning models such as NMT, GAN, VAE, and AAE, the distribution of generated molecules approximates the distribution of their training data. The magenta triangles and blue diamonds indicate real molecules in ChEMBL[34] database, which have extrapolated properties from MOSES training data distribution.

desired materials from unconditional generative models, such as generative adversarial networks (GANs)[27] and variational autoencoders (VAEs)[28]. These approaches use additional methods to find appropriate latent code, which is required to generate the target-hitting materials. Navigating policies of latent space trained by reinforcement learning (RL)[29, 30] and optimization techniques[31, 32] belong here.

Unfortunately, all of the previously mentioned models (NMT, GAN, and VAE-based) are difficult to use in materials extrapolation for discovering novel materials with properties that are out of training data distribution (Fig. 1). To generate realistic molecules with these models, the models should be trained to generate molecular data that approximate the probability distribution of the chemical system. However, since it is impossible to know the true probability of the chemical system, the models are trained to generate data that approximate the empirical probability of the training data. Hence, the *probability distribution-learning models* are not suitable for generating materials in regions with little or no known data (such as materials extrapolation). In addition, there are several ongoing discussions about whether probability distribution-learning models are suitable for extrapolation problems[9, 10, 33].

Combinatorial chemistry[35] was invented in the 1980s and can generate molecules with properties out of known data. These types of methods use a set of molecular fragments and rules for fragment combination. Breaking of retrosynthetically interesting chemical substructures (BRICS)[36] is an example of combinatorial chemistry. This technique involves combining randomly selected BRICS fragments with their template-based fragment combination rules, which is similar to assembling Lego blocks. Therefore, combinatorial chemistry can create all physically possible molecular structures that can be

obtained from the combination of molecular fragments. According to our estimation, approximately  $4 \times 10^{16}$  types of small molecules ( $\leq 500$  Da) can be combined with 2,207 BRICS fragments. Considering that the total number of small molecules is known to be  $10^{60}$ [37], this means that it can cover a fairly wide area. However, there is the limitation that the combinatorial chemistry-based molecular generator does not know which molecular fragments to be selected to complete the desired material. In other words, it has no policy to guide the selection of molecular fragments to obtain the target material. Hence, it proceeds with countless attempts to combine randomly selected fragments and selects the best compound from the generated material candidates, which can result in a combinatorial explosion[38]. If we assume that it takes 1 s to assemble one molecule, it would take  $1.27 \times 10^9$  years to enumerate all possible small organic molecules using 2,207 molecular fragments;  $4 \times 10^{16}$  molecules  $\times 1$  second =  $1.27 \times 10^9$  years.

Herein, we introduce RL to provide combinatorial chemistry with a molecular fragment selection policy that guides the generating molecule towards the target. With a randomly selected initial fragment, the AI-driven policy iteratively selects the next fragment to be combined. In the training phase, the policy is learned by giving a higher reward if the properties of the generated molecule are closer to the target. Therefore, the learned policy enables an efficient search of chemical space and helps to escape from the combinatorial explosion problem by providing direction to the target. Moreover, the proposed model—*AI-driven combinatorial chemistry*—enables materials extrapolation, which is impossible for probability distribution-learning models. To demonstrate this concept empirically, we apply AI-driven combinatorial chemistry and two probability distribution-learning models to a discovery problem of extreme materials that hit multiple target properties simultaneously. The results indicate that our model can discover extreme target materials that probability distribution-learning models cannot reveal. Furthermore, we theoretically demonstrate why the probability distribution-learning models are not suitable for problems involving materials extrapolation. To illustrate the performance in actual problems, we conduct two practical experiments on materials extrapolation. The first is to discover protein docking materials to a 5-hydroxytryptamine receptor 1B (5-HT<sub>1B</sub> receptor) with high binding affinity. The second is the discovery of human immunodeficiency virus (HIV) inhibitors with high potency. These two experiments demonstrate that the proposed model can solve various problems involving materials extrapolation.

## 2 Results

### 2.1 Theoretical review of probability distribution-learning models

Inverse molecular design models based on NMT, VAE, and GAN learn the empirical probability distribution of training data  $P_{data}$ . Let  $X, Y = (X_1, Y_1), \dots, (X_N, Y_N)$  denote  $N$ -sampled training data. Here,  $X_i =$

$(x_{i,1}, \dots, x_{i,T'})$  denotes sequence data of the  $i$ -th molecular structure, and  $Y_i = (y_{i,1}, \dots, y_{i,T})$  denote a set of properties of the  $i$ -th molecule. The NMT-based models are trained to translate the input  $Y_i = (y_{i,1}, \dots, y_{i,T})$  into a paired output sequence  $X_i = (x_{i,1}, \dots, x_{i,T'})$ . Here,  $x_{i,t}$  is a one-hot encoded vector of the  $t$ -th token constituting a molecule  $X_i$ . The  $\theta$ -parameterized translator  $G_\theta^{NLP}$  should be trained to select a token  $x_{i,t}$  iteratively over  $t = 1, \dots, T'$ , by maximizing the likelihood  $\prod_{i=1}^N \prod_{t=1}^{T'} G_\theta^{NLP}(x_{i,t} | Y_i, x_{i,1:t-1})$  empirically. The actual training process is conducted by minimizing its negative log-likelihood  $-\sum_{i=1}^N \sum_{t=1}^{T'} \log G_\theta^{NLP}(x_{i,t} | Y_i, x_{i,1:t-1})$ , which is equivalent to minimizing cross-entropy  $H(\cdot, \cdot)$  of hypothesis  $\hat{X}_\theta$  from training data  $X$ :

$$\begin{aligned} H(X, \hat{X}_\theta) &= - \sum_{i=1}^N \sum_{t=1}^{T'} P(X) \log P(\hat{X}_\theta) \\ &= H(X) + D_{KL}(P(X) \parallel P(\hat{X}_\theta)) \end{aligned} \quad (1)$$

where  $H(X) = -\sum_{i=1}^N \sum_{t=1}^{T'} P(X) \log P(X)$  denotes the entropy[39] of training data  $X$ , and  $D_{KL}(P(X) \parallel P(\hat{X}_\theta))$  is the Kullback–Leibler (KL) divergence[40] of hypothesis probability  $P(\hat{X}_\theta)$  from  $P_{data}$ . Since  $H(X)$  is not a function of trainable parameter  $\theta$ , minimizing the cross-entropy  $H(X, \hat{X}_\theta)$  is equivalent to minimizing the KL divergence term in Equation (1). Thus, the optimal  $G_\theta^{NLP}$  is obtained by approximating  $P(\hat{X}_\theta)$ —which is the probability distribution of data generated by  $G_\theta^{NLP}$ —to  $P_{data}$ . It means that  $G_\theta^{NLP}$  learns the empirical probability distribution of training data  $P_{data}$ , not the true probability distribution of the system  $P$ .

Second, VAE-based models are types of generative self-learning models that learn the empirical probability distribution of training data  $P_{data}$ . The models are trained to encode training data  $X = X_1, \dots, X_N$  in the latent space with encoder  $Q_\phi^{VAE}$  and reconstruct it with decoder  $G_\theta^{VAE}$ . The difference from autoencoders is that the latent variables  $z$  are constrained to follow a prior distribution such as normal distribution. The VAEs are trained using the following objective function[28]:

$$\operatorname{argmin}_{\phi, \theta} \sum_{i=1}^N -\mathbb{E}_{Q_\phi^{VAE}(z|X_i)} [\log G_\theta^{VAE}(X_i | z)] + D_{KL}(Q_\phi^{VAE}(z | X_i) \parallel P(z)) \quad (2)$$

When looking at the VAEs from the perspective of a generative model, the KL divergence term simply acts like a regularizer in the training process. The expectation term measures the reconstruction error of  $G_\theta^{VAE}$  and it is approximated by using the following  $L$ -number of Monte-Carlo sampling:

$$-\mathbb{E}_{Q_{\phi}^{VAE}(z|X_i)} [\log G_{\theta}^{VAE}(X_i | z)] \approx -\frac{1}{L} \sum_{z_j=1}^L \log (G_{\theta}^{VAE}(X_i | z_j)) \quad (3)$$

Here, the approximated reconstruction error term is a form of negative log-likelihood over training data  $X$ . Hence, it is equivalent to minimizing the cross-entropy  $H(\cdot, \cdot)$  of hypothesis  $\hat{X}_{\theta,z}$  from training data  $X$ :

$$\begin{aligned} H(X, \hat{X}_{\theta,z}) &= - \sum_{i=1}^N \sum_{t=1}^{T'} P(X) \log P(\hat{X}_{\theta,z}) \\ &= H(X) + D_{KL} \left( P(X) \parallel P(\hat{X}_{\theta,z}) \right) \end{aligned} \quad (4)$$

As mentioned above, this is also equivalent to minimizing the KL divergence term in Equation (4), since  $H(X)$  is not a function of trainable parameter  $\theta$ . Hence, the optimal  $G_{\theta^*}^{VAE}$  is obtained by approximating the probability distribution of hypothesis  $P(\hat{X}_{\theta,z})$  to the  $P_{data}$ . This means that  $G_{\theta}^{VAE}(X | z)$  with  $z \sim Q_{\phi}^{VAE}(z | X)$  approximates  $P_{data}$ .

Third, GAN is also a model to obtain a generator  $G_{\theta}^{GAN}$  that approximates  $P_{data}$ . Here,  $G_{\theta}^{GAN}$  learns the  $P_{data}$  in the learning process to generate data that sufficiently resembles training data  $X$  to deceive the discriminator  $D_{\phi}^{GAN}$ . Note that it has been proved that the global minimum of the virtual training criterion of the generator is achieved if (and only if)  $P_{data} = G_{\theta}^{GAN}(z)$  [27]. This means that the optimal  $G_{\theta^*}^{GAN}$  is obtained by approximating the hypothesis probability  $P(\hat{X}_z)$  to the probability of training data  $P_{data}$ .

Therefore, it can be concluded that models based on NMT, VAE, and GAN used for inverse molecular design are models to derive an approximator of  $P_{data}$ . Unfortunately, since  $P_{data}$  derived from the observed empirical data is not equal to the true probability  $P$ , it cannot guarantee that the probability-distribution learning models will work well for problems involving materials extrapolation.

## 2.2 AI-driven combinatorial chemistry with BRICS

The AI-driven combinatorial chemistry, illustrated in Fig. 2 is universally applicable to a variety of material discovery tasks, by designing a target molecule with a randomly selected molecular fragment. A trained AI-driven policy iteratively selects the next fragment to be combined. Here, the AI-driven policy serves as a guide to generate a target-hitting molecule. This approach has three main phases: configuration settings (Fig. 2c-f), training (Fig. 2a,b), and inference (Fig. 2h,i).

In the configuration settings phase, all settings necessary for reinforcement learning are customized. Accordingly, the task for materials discovery must

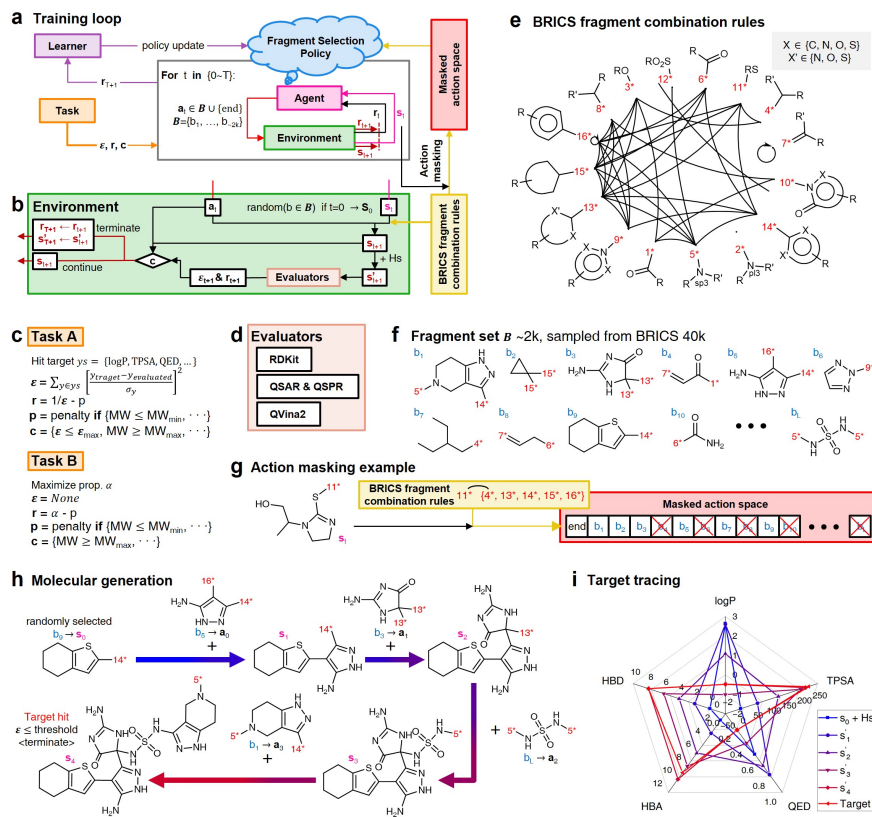


**Fig. 2 Overview of AI-driven combinatorial chemistry with BRICS.** **a** Training loop. Depending on the given task, target error function  $\epsilon$ , rewards  $r$ , and termination conditions  $c$  are designed. Each episode involves a maximum of  $T$  iterations of selecting and combining molecular fragments. If one of termination condition  $c$  is met, the process is terminated early before reaching the maximum step  $T$ . In this process, the model learns a policy that selects a molecular fragment  $a_t$  to bind to the molecule at step  $t$  ( $s_t$ ) to maximize the final reward  $r_{T+1}$ . **b** Environment at step  $t$ . To evaluate a molecular property, the tested molecule must not have unfilled binding sites. Accordingly, hydrogen is attached to the remaining binding sites of the combined molecule  $s_{t+1}$ . Here,  $s'_{t+1}$  denotes a potential output molecule at step  $t$ . **c** Two types of tasks. Task A refers to a task to find multiple target-hitting molecules. Task B refers to a task to find a molecule that maximizes a property. **d** Types of evaluators. **e** Modified BRICS[36] fragment combination rules. Here, the RDKit[41] version 2020.09.1.0 of the modified BRICS rules is adopted. There are 16 templates of BRICS molecular fragments with unique binding sites (colored red). The fragment template with 2\*-binding site is removed in the modified version. This figure is modified from Degen et al., 2008, *ChemMedChem*, 10(3): 1503-1507[36], with permission of Wiley-VCH GmbH. **f** Fragment set  $B$ . Here,  $B \cup \{end\}$  is defined as action space. **g** Action masking example. An example of generating a target-hitting molecule is shown in **h** and **i**.

be specified. There are two types of tasks for this (Fig. 2c): the discovery of materials to hit the multiple target properties (Task A), and the discovery of materials to maximize or minimize a specific property (Task B). Depending on the type of given task, the user designs the reward function  $r$ , target error

function  $\varepsilon$ , and termination conditions  $c$ . The reward function  $r$  is designed to give a higher reward the better a given task is performed. For Task A, the target error function  $\varepsilon$  and reward function  $r$  are designed as sum errors for the multiple target properties and the reciprocal of the target error function  $\varepsilon$ , respectively. In the case of Task B, the property itself is used as the reward function  $r$ ; hence, maximizing  $r$  is equivalent to maximizing the property. For the minimization case of Task B, the negative property is used as the reward function  $r$ . We can also consider the constraints  $p$ , which are reflected in the reward function  $r$  by giving penalties if one of the constraints  $p$  is not satisfied. Here, the minimum molecular weight ( $MW_{min}$ ) and minimum number of fragments ( $n_{min}$ ) that make up a molecule can be used as constraints  $p$ . These enable the model to generate various molecules by preventing premature termination, which would cause the generation of molecules that were too small and uniform.

The termination conditions ( $c$ ) pertain to deciding when to terminate the process of selecting and combining additional molecular fragments, which determines the characters of the final output molecule. Hence, the termination conditions  $c$  are designed considering the given task. The molecular generation process is terminated early if one of the termination conditions  $c$  is satisfied. Accordingly, the maximum target error ( $\varepsilon_{max}$ ), maximum molecular weight ( $MW_{max}$ ), and maximum number of fragments ( $n_{max}$ ) are used to design the termination conditions ( $c$ ). It should be noted that the process is also terminated if there are no more sites for binding fragments to the combined molecule at step  $t$  ( $s_{t+1}$ ) or if the action at step  $t$  ( $a_t$ ) is the *end* action. These are also included in the termination conditions  $c$ .

To evaluate the previously mentioned functions and conditions, the evaluators for the interesting properties (Fig. 2d) are utilized selectively to calculate the properties of potential output molecule at step  $t$  ( $s'_{t+1}$ ). Here,  $s'_{t+1}$  is a molecule derived by attaching hydrogen to the unfilled binding sites of the combined molecule at step  $t$  ( $s_{t+1}$ ) if  $s_{t+1}$  has any unfilled binding site (See Fig. 2b). Here, RDKit[41] was used selectively to evaluate the calculated octanol-water partition coefficient ( $\log P$ )[42], topological polar surface area (TPSA)[43], quantitative estimates of drug-likeness (QED)[44], number of hydrogen bond acceptors (HBA), number of hydrogen bond donors (HBD), and molecular weight (MW). A quantitative structure-activity relationship (QSAR) model[22] and QVina2[45]—, which is a tool for discovering the minimum-energy docking conformation of a tested molecule and calculating its docking score, are also selectively used to evaluate drug activity for dopamine receptor D2 (DRD2) and the binding affinity to the 5-HT<sub>1B</sub> receptor, respectively.

For combinatorial chemistry, fragment set  $B$  and its combination rules should be set. Accordingly, a modified version[41] of the BRICS[36] system was adopted (Fig. 2e,f). Since the best performance was achieved for approximately 2k action spaces in the preliminary experiments (Supplementary Note 2), approximately 2k fragments were sampled from BRICS 40k for fragment

set  $B$ . The BRICS fragment combination rules are rules to bind 16 molecular templates, where each template has a unique binding site (red digit in Fig. 2e).

In the training phase, our model was trained using the proximal policy optimization (PPO) algorithm[46], which is known to perform well in RL problems with discrete actions. This is because it has the advantages of stable training, sample efficiency, scalability, and flexibility. In the preliminary experiments, PPO performed optimally for our problem among several state-of-the-art RL algorithms (Supplementary Note 3). An episode iteratively proceeds the process of selecting and combining molecular fragments from steps 0 to  $T$  (Fig. 2a). If one of the termination conditions  $c$  is satisfied, the episode is prematurely terminated at the step (Fig. 2b). At step 0, an episode is started with a randomly selected fragment  $s_0$ , and the randomness makes the final output molecule  $s'_{T+1}$  various. Subsequently, action masking is performed, which masks the actions that are not applicable to  $s_0$ . Fig. 2g displays an example of action masking at step  $t$ , in which molecule  $s_t$  has an unfilled binding site of 11\*. As shown in Fig. 2e, the 11\*-binding site can bind to the 4\*, 13\*, 14\*, 15\*, and 16\*-binding sites. Hence, blocks  $b_4, b_6, b_8, b_{10}, \dots, b_L$  that do not have any binding sites of 4\*, 13\*, 14\*, 15\*, and 16\* are masked. Thereby, the fragment selection policy is enforced not to select the masked actions. This action masking helps to generate molecules that do not violate the chemical valence rule and enables efficient learning by reducing the action space. In this way, the fragment selection policy selects an action at step 0 ( $a_0$ ) from the unmasked actions.

If the selected action at step  $t$  ( $a_t$ ) is the *end*-action, the molecule at step  $t$  ( $s_t$ ) becomes  $s_{t+1}$  (Fig. 2b). Moreover, if  $a_t$  is a fragment,  $a_t$  is combined with  $s_t$  to make a combined molecule at step  $t$  ( $s_{t+1}$ ). To evaluate the properties of a molecule, the molecule should not have any unfilled binding sites. Hence, the potential output molecule at step  $t$  ( $s'_{t+1}$ ) is derived by attaching hydrogen to the remaining binding site of  $s_{t+1}$ . Then, the interesting properties of  $s'_{t+1}$  are evaluated to obtain the target error  $\varepsilon_{t+1}$  and reward  $r_{t+1}$  at step  $t$ . Now, to check whether one of the termination conditions  $c$  is satisfied,  $a_t$ ,  $\varepsilon_{t+1}$ , and  $r_{t+1}$  are considered. If one of the termination conditions  $c$  is satisfied, the reward  $r_{t+1}$  and the potential output molecule  $s_{t+1}$  at step  $t$  are treated as the final reward  $r_{T+1}$  and the final output molecule  $s'_{T+1}$ , respectively. Then, the episode is terminated and the learner updates the fragment selection policy with  $r_{T+1}$  (Fig. 2a,b). If any of the termination conditions  $c$  are not satisfied, the environment outputs the combined molecule  $s_{t+1}$ . Then, the model iteratively proceeds to the next step of the process until either one of the termination conditions  $c$  is satisfied or the maximum step  $T$  is reached. This process is repeated for a preset number of iterations to train the model.

After the training is completed, the trained policy is used to generate a target molecule in the inference phase. Fig. 2h,i displays an example of molecular generation, in which new molecular fragments are selected and combined to complete a target molecule from steps 0 to 3. In the process, the properties of the generated potential output molecules ( $s'_1$  to  $s'_4$ ), which are derived from

**Table 1** The target-hitting errors for materials interpolation

	$RMSE_i$		$\overline{RMSE_i}^a$
	cRNN[22]	GCT[21]	Average
logP	0.379	0.368	0.373
TPSA	5.476	5.109	5.292
QED	0.081	0.075	0.078
HBA	0.932	1.204	1.068
HBD	0.223	0.247	0.235
MW	5.954	8.272	7.113
DRD2	0.113	0.098	0.105

<sup>a</sup> $\overline{RMSE_i}$  refers average  $RMSE$  of target property  $i \in \{\log P, \text{TPSA}, \text{QED}, \text{HBA}, \text{HBD}, \text{MW}, \text{DRD2}\}$  for cRNN[22] and GCT[21].

hydrogen attachment of the combined molecules ( $s_1$  to  $s_4$ ), change from the properties of a randomly selected molecular fragment ( $s_0$ ) to the target properties (logP:  $-0.488$ , TPSA:  $220.83$ , QED:  $0.207$ , HBA:  $9$ , HBD:  $8$ ). In step 3, the properties of the potential output molecule  $s'_4$  (logP:  $-0.488$ , TPSA:  $211.09$ , QED:  $0.205$ , HBA:  $10$ , HBD:  $8$ ) are close to the target properties (Fig. 2h). Since the target error  $\varepsilon_4$  is lower than the maximum target error  $\varepsilon_{max}$ , the process is terminated at step 3. Hence, the potential output molecule at step 3 ( $s'_4$ ) becomes the final output molecule.

## 2.3 Materials extrapolation to hit multiple extreme target properties

In this section, we empirically demonstrate that AI-driven combinatorial chemistry enables materials extrapolation, which is not possible with probability distribution-learning models. To achieve this, we adopt two different types of probability distribution-learning models and compare their performance with our model in terms of materials extrapolation. One of the adopted models is a conditional recurrent neural network (cRNN)[22] (an NMT-based translator), while the other is the generative chemical transformer (GCT)[21] (a cVAE-based generative model).

For the demonstration, we conducted experiments on generating molecules to hit multiple target properties. The experimental setup was borrowed from ref. [22]. In the experiments, the following seven drug-related target properties were given to the models to generate target-hitting molecules: logP, TPSA, QED, HBA, HBD, MW, and DRD2. Detailed information about the properties is summarized in Methods 4.1. Here, RDKit and a QSAR model for DRD2[22] were adopted as evaluators.

First, the original performances of cRNN[22] and GCT[21] were evaluated to demonstrate how their performance degraded on materials extrapolation. The two models were trained and tested with data sets[22] curated from the ChEMBL database[34]. Here, the original performance means how well target-hitting molecules were generated for the given target properties C0—which

were gathered from 149,679 molecules in the curated ChEMBL test data[22]. For each of the 149,679 C0 targets, a molecular generation was tried with cRNN and GCT. Since the distributions of the test and training data were similar, the original performance evaluated for the test data could be considered the same as the performance for *materials interpolation*.

To conduct the experiments on materials extrapolation, we adopted another molecular dataset with properties that were more widely distributed than the trained data[22]: PubChem SARS-CoV-2 clinical trials [47] (Fig. 3a). Among the molecules in this dataset, 10 molecules were sampled whose properties were outside the trained data, which were then set as the extrapolated targets (C1 to C10). Since these 10 molecules were real molecules that exist in the real world, their properties would be physically feasible targets to generate. For each extrapolated target, 10,000 molecular generations were tried with cRNN[22] and GCT[21].

To evaluate the performance of generating molecules that hit multiple target properties, the criteria for determining whether each target property was hit should be defined. Accordingly, in the experiment of materials interpolation with cRNN[22] and GCT[21], the root mean squared error of each target property  $i$  ( $RMSE_i$ ) was analysed (Table 1). Since all  $RMSE_i$  for cRNN and GCT were not significantly different from each other, we determined that the magnitude of the average  $RMSE_i$  ( $\overline{RMSE_i}$ ) represents the difficulty of generating molecules that hit the target property  $i$ . Therefore, by setting  $\pm\overline{RMSE_i}$  as the target bound of  $i$ , a wide bound was assigned to targets that were difficult to hit and a narrow bound was assigned to any targets that were easy to hit. Furthermore, we introduced a relative error measurement metric ( $pRMSE_i$ ), as follows:

$$pRMSE_i = \frac{|y_i - \hat{y}_i|}{\overline{RMSE_i}} \quad (5)$$

where  $y_i$  and  $\hat{y}_i$  refer to the target property  $i$  and the evaluated property  $i$  of a generated molecule, respectively. To assess the overall performance of discovering target-hitting molecules, we also introduced the following aggregated scoring metric *score*

$$score = \frac{1}{\sum_i pRMSE_i} \quad (6)$$

Fig. 3b displays the results for materials interpolation (targets C0) and extrapolation (targets C1 to C10). Since the number of attempted molecular generations for materials interpolation and extrapolation were different, the rescaled results based on 10,000 trials are summarized in the left-hand side of Fig. 3b for comparison. For materials interpolation (targets C0 in Fig. 3b), the cRNN[22] generated 3,479 molecules that hit all of the seven targets (logP, TPSA, QED, HBA, HBD, MW and DRD2) simultaneously and 4,453 molecules hit the five targets (logP, TPSA, QED, HBA, and HBD) simultaneously. With the same criteria, the GCT[21] generated 2,664 molecules that hit all seven targets and 3,994 molecules hit the five targets simultaneously. These

12

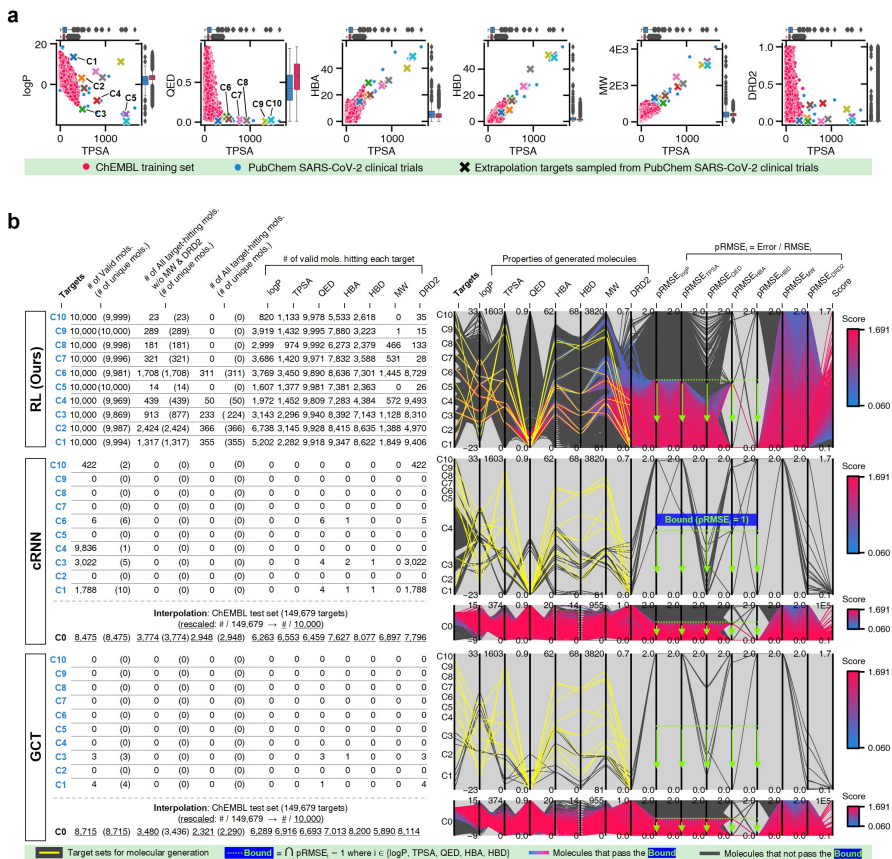


**Fig. 3 Experimental results for generating multiple target-hitting molecules. a** Distribution of the curated ChEMBL training data[22] and the extrapolation targets C1 to C10. **b** Results comparison of AI-driven combinatorial chemistry, cRNN[22], and GCT[21]. The left-hand side table shows the number of molecules that hit the target bounds. The blue-colored lines in the right-hand side parallel coordinates plot indicate materials within the green target bounds of logP, TPSA, QED, HBA, and HBD simultaneously. The blue-red colored lines were colored according to the log-scaled aggregated score. The 10 yellow lines indicate the target properties of the 10 targets.

results confirmed that both models were able to generate hit-like materials in the trained region.

Both probability distribution-learning models achieved poor results in terms of molecular extrapolation. For each target from C1 to C10 outside the trained data, we conducted 10,000 trials to generate the molecules per target. As displayed in the results for the targets C0 to C10 of Fig. 3b, both the probability distribution-learning models failed to generate molecules that hit all of the targets and did not generate molecules that hit the five targets. Even GCT[21] only succeeded in generating seven valid and unique molecules that satisfied the chemical valence rule out of 100,000 trials, with four and three

molecules being generated for targets C1 and C3, respectively. In comparison, cRNN[22] generated 15,068 chemically valid molecules, although only 21 were unique. In particular, 15,054 out of the 15,068 valid molecules were nonsensical outcomes that were overlapped and too small, such as  $CH_4$ ,  $CH_4S$ ,  $H_2O$ ,  $H_2S$ ,  $SO$ ,  $H_2OS$ , and  $H_2S_2$ . Considering that the target MWs of C1 to C10 were distributed in the range of 1,026 to 3,124 *Da*, it was difficult to determine whether it operated correctly. Moreover, other generated molecules exhibited considerable deviations from the intended targets. Detailed information on the generated molecules is summarized in Supplementary Table 1-4.

For targets C1, C2, C3, C4, and C6, our AI-driven combinatorial chemistry generated 1,315 target-hitting molecules that hit all seven targets simultaneously. Here, 355, 366, 233, 50, and 311 molecules that hit all targets were generated for the targets C1, C2, C3, C4, and C6, respectively. For targets C5, C7, C8, C9, and C10, AI-driven combinatorial chemistry could not generate molecules that hit all targets. However, it successfully generated 828 molecules that hit five targets that failed with the probability distribution-learning models. Here, 14, 321, 181, 289, and 23 molecules that hit five targets were generated for targets C5, C7, C8, C9, and C10, respectively. In addition, all of the generated molecules were chemically valid.

Also, in fact, it is hard to assert that it completely failed to hit the seven target properties simultaneously for the targets C5, C7, C8, C9, and C10. For these targets, the generated molecules exhibited lower *pRMSEs* (see *pRMSEs* of RL displayed in Fig. 3b). This means that if the target bounds were more broadly set, there would be more molecules that were counted as molecules that hit all targets. It should be noted that the employed MW target bound  $\pm 7.113$  *Da* and DRD2 target bound  $\pm 0.105$  were fairly narrow (Table 1). The target bound of MW 7.113 *Da* was so small that it was less than one atom apart. Furthermore, the target bound of DRD2 was considerably smaller than the commonly known drug activity prediction accuracy of QSAR models. In [22], the QSAR model for DRD2 was used as a binary classifier to evaluate as either active (when the predicted value was  $\geq 0.5$ ) or inactive ( $\leq 0.5$ ). For this reason, we believe that the number of molecules hitting the targets MW and DRD2 was less counted than the number of molecules hitting the other targets (See MW-axis and DRD2-axis of RL in the left-hand side Table of Fig. 3b). Hence, we conducted a supplementary experiment on another dataset to generate five target-hitting molecules that excluded for MW and DRD2 (Supplementary Note 1). As a result, we confirmed that our model successfully generated molecules with extreme properties outside the known materials, which is not possible with probability distribution-learning models.

## 2.4 Application to the discovery of protein docking materials

The discovery of small molecules that dock to a target protein is a practical problem in drug discovery. Moreover, binding affinity to a target receptor is an important indicator for measuring drug-target interactions[3]. Since materials

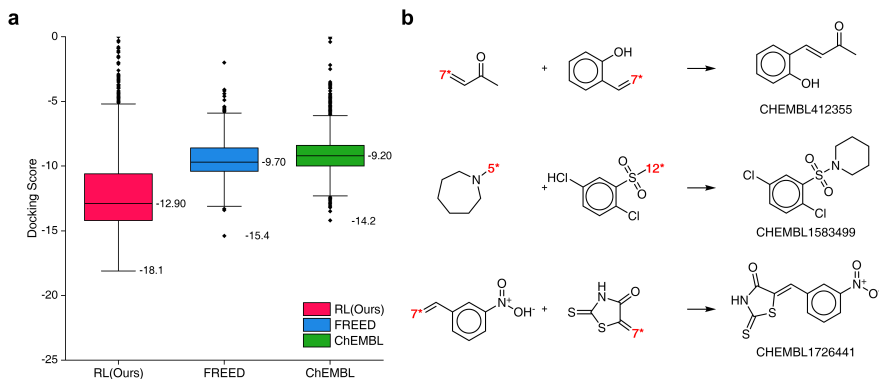


**Fig. 4 Generated 5-HT<sub>1B</sub> receptor docking materials.** **a** Comparison of docking scores for the three molecular sets. The red color indicates the docking scores of 10,000 generated molecules from AI-driven combinatorial chemistry. The green color indicates the docking scores of 10,000 drug-like molecules that were randomly sampled from ChEMBL[34] database. The blue color indicates the docking scores of 1,871 molecules generated by FREED[2], which has been reported in the paper. The 1,871 molecules have been reported as de novo cases with 4-step in their paper. Note that the maximum number of fragments constituting a compound is the same as ours. The docking scores of the 1,871 molecules were re-evaluated using QVina2[45] under the same calculation configuration as ours. **b** Three molecular examples that were generated by AI-driven combinatorial chemistry, which exactly matched with active drug molecules reported in the PubChem Bioassay database[49].

with higher binding affinity to the target protein (compared to other proteins) can be considered as having high selectivity and docking ability, the discovery of materials that maximize target binding affinity is a key objective in protein docking drug discovery[48]. Along with the previous experiment, maximizing the binding affinity is one of the material-extrapolation problems for discovering better materials.

In this section, we demonstrate that AI-driven combinatorial chemistry can discover materials that maximize the binding affinity towards the 5-hydroxytryptamine receptor 1B (5-HT<sub>1B</sub> receptor), which is related to mental diseases. A detailed description of the 5-HT<sub>1B</sub> receptor is summarized in Methods 4.1. We adopted QVina2[45] (a molecular docking simulator) to discover the minimum-energy docking conformation. This simulator evaluates the docking score fast and reliably. Since the docking score is an indicator that is inversely proportional to the binding affinity, the reward function was set as the negative docking score.

To evaluate the performance of AI-driven combinatorial chemistry, the docking scores of 10,000 generated molecules from our model were compared with the docking scores of two other molecular sets. One was a set of 1,871 molecules that were generated to maximize the negative docking score towards the 5-HT<sub>1B</sub> receptor using fragment-based generative RL with explorative experience replay for drug design (FREED)[2], which is reported in the paper. The other set was 10,000 molecules that were randomly sampled from ChEMBL[34] drug-like molecules. The docking scores of the three sets

are summarized in Fig. 4a, which were calculated with QVina2. The calculation configuration is described in Supplementary Note 4. The best molecule with the lowest docking score was discovered from our model and the median docking score for the sets was also the lowest.

To check if potential drug molecules were found among the 10,000 generated molecules, we investigated whether any generated molecules were an exact match with the drug-like molecules in the ChEMBL[34] database. There were 23 molecules whose molecular structures exactly matched with real drug-like molecules in the ChEMBL database, of which 13 out of the 23 molecules had labels on drug activity (active or inactive). It should be noted that the number of small organic molecules reached approximately  $10^{60}$ [37], of which only  $2.2 \times 10^6$  were included in the ChEMBL database[34]. Hence, it was difficult to find molecules with an exact match. An interesting finding is that five (CHEMBL1583499, CHEMBL1726441, CHEMBL412355, CHEMBL2261013, and CHEMBL99068) of the 13 molecules had been reported as active for some targets. Among these, three (CHEMBL1583499, CHEMBL1726441, and CHEMBL412355) were active in the related roles in which the 5-HT<sub>1B</sub> docking materials have been reported to have an effect. For example, CHEMBL1726441 is reported to be active for various targets such as Corticotropin-releasing factor receptor 2, Rap guanine nucleotide exchange factor 4, Nuclear factor erythroid 2-related factor 2, and Geminin. These targets have been reported to act in the human brain and peripheral tissues, playing a psychopathological role[50] and controlling brain function[51]. These investigations were conducted with the PubChem Bioassay database[49]. The other investigated results are summarized in Supplementary Table 7.

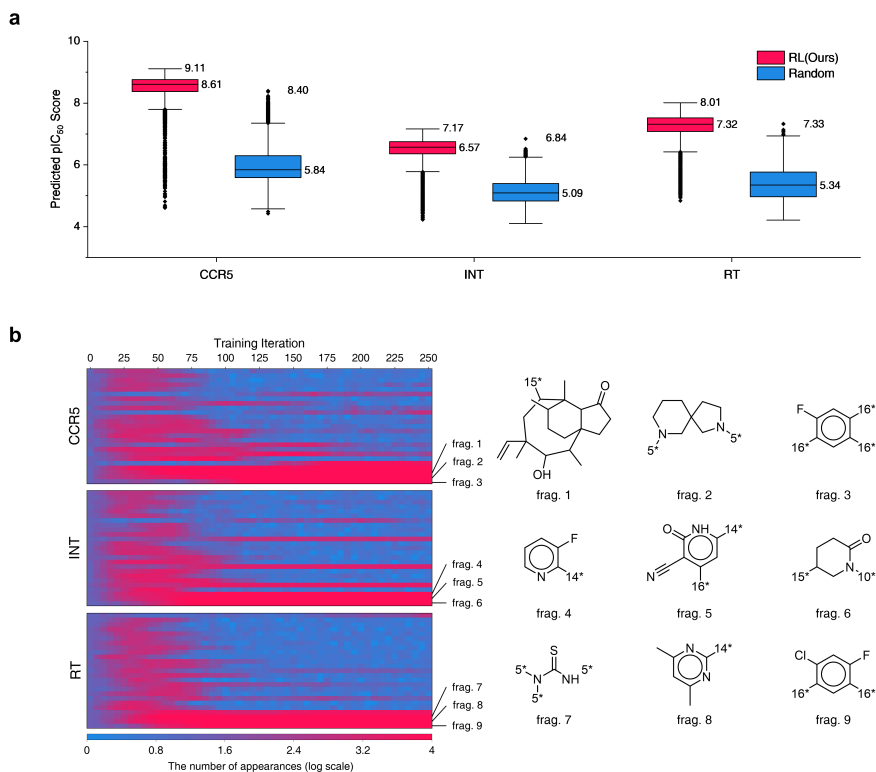
## 2.5 Application to discovery of HIV inhibitors

This section describes experiments in which AI-driven combinatorial chemistry was applied to discover HIV inhibitors. Here, we selected three HIV inhibition targets: C-C chemokine receptor type 5 (CCR5), HIV integrase (INT), and HIV reverse transcriptase (RT). Detailed information about the targets is summarized in Methods 4.1. To evaluate the HIV inhibition potency of molecules, pIC<sub>50</sub> predictors[4] for the three HIV inhibition targets were adopted. It should be noted that pIC<sub>50</sub> is equal to  $-\log IC_{50}$ , where IC<sub>50</sub> is an indicator that measures the amount of a particular inhibitory substance required to inhibit a given biological process or biological component by 50%. In other words, the lower the value of IC<sub>50</sub>, the higher the HIV inhibition potency. Moreover, the higher the value of pIC<sub>50</sub>, the higher the HIV inhibition potency. Therefore, we set pIC<sub>50</sub> as the reward function to make our model discover HIV inhibitors with high potency.

In total, 10,000 generated molecules from our model were compared with the same number of molecules randomly combined by no-policy combinatorial chemistry (Fig. 5a). For all the HIV inhibition targets, molecules generated by our model exhibited significantly higher pIC<sub>50</sub> values compared to those of random combination without a policy (original combinatorial chemistry).

This result indicated that our model learned the fragment-selection policy to discover the intended materials. The benchmark results compared to the other six generators for HIV inhibitors are summarized in Supplementary Table 9, in which our model achieved the highest  $\text{pIC}_{50}$  values for targets CCR5 and RT.

To analyze the policy change of molecular fragment selection in the training phase, we generated 10,000 molecules at the end of every training iteration. The derived frequencies for 25 fragments with the biggest change (how many molecules had the fragment) are plotted on the left of Fig. 5b. In the initial state (where no policy was learned), the frequency of all fragments was similar. As the training progressed, the frequency of each fragment became varied. Although the selected frequency of some fragments increased as training proceeded, some of them decreased at certain points. This is because the agent



found the combinations of molecular fragments that provided a high reward. Hence, the selection of other fragments that did not have any merit in the pIC<sub>50</sub> score rapidly decreased. The most selected fragments differed according to the type of HIV inhibition targets. Since the fragments were most often used to maximize the pIC<sub>50</sub> for each target, we believe they may be key structures for HIV inhibitors on each target.

### 3 Conclusion

From a data science perspective, the discovery of better than previously known is to find materials with properties outside outliers—materials extrapolation. Most of the reported inverse molecular design models are based on data probability distribution-learning models, such as machine translators and generative models (including Seq2Seq[23], Transformer[24], GAN[27], and VAE[28]). However, these models are too limited for use in materials extrapolation, which requires generating materials in the untrained area. To solve this problem, we adopted combinatorial chemistry[35], which generates molecules from combinations of randomly selected molecular fragments. Fundamentally, it is a rule-based data-free molecular designer for generating all physically possible molecular structures that can be obtained from the combination of molecular fragments. However, since the lack of a molecular fragment selection policy can cause a combinatorial explosion[38], RL is applied to train its fragment-selection policy to provide a direction toward target materials.

This paper contains three major contributions. First, we theoretically demonstrated that most inverse molecular design models based on probability distribution-learning of data are too limited for use in materials extrapolation. Second, we empirically demonstrated that our proposed AI-driven combinatorial chemistry works well on various problems of materials extrapolation, such as the discovery of multiple target-hitting materials, protein docking materials, and HIV inhibitors. This demonstrated that our model could be applied universally in various problems pertaining to materials extrapolation. Third, the limitations of our model were also analysed (Methods 4.8). One of these was that re-training would be required if the target was changed. The other limitation was a sparse reward problem that interrupted the discovery of materials with extreme properties. However, since studies to solve these limitations have already been reported, we plan to address these issues in future studies.

Furthermore, since the BRICS[36] system is designed based on drug-like materials, our applications were limited to drug discovery. Therefore, we plan to extend our approach to various problems of discovering better materials in the fields of OLEDs, battery materials, and polymers.

## 4 Methods

### 4.1 Molecular Descriptors

For the experiment in materials extrapolation, where the aim was to hit multiple extreme target properties, seven properties were set: logarithm of the calculated octanol-water partition coefficient (logP)[42]; topological polar surface area (TPSA)[43]; quantitative estimate of drug-likeness (QED)[44]; number of hydrogen bond acceptors (HBA); number of hydrogen bond donors (HBD); molecular weight (MW); and drug activity for dopamine receptor D2 (DRD2). Each property is considered important in the field of drug discovery. The term logP is a descriptor for the lipophilicity of a molecule, which refers to a molecule's capacity to dissolve in fats or oils. This is an important property in drug design since it has an impact on the molecule's capacity for penetrating cell membranes and reaching its intended target. The term TPSA is a calculated descriptor of the polar surface area (PSA) of a molecule, which refers to the area of a molecule having polar functional groups that could form hydrogen bonds with water molecules. A molecule is less polar and more likely to be able to penetrate cell membranes if it has a lower PSA value. The terms HBA and HBD are also important properties in drug design because they can affect a molecule's capacity to interact with other molecules through hydrogen bonding. Hydrogen bonding is frequently used in drug design to facilitate the binding of a molecule to the target receptor. Moreover, hydrogen bonding can affect a drug molecule's solubility and permeability, which influence its pharmacological properties. Term MW is a descriptor used in drug discovery, as it can affect a drug's pharmacokinetics, efficacy, and safety. This is because the size of the molecules can influence a drug's absorption, distribution, metabolism, or degree of penetration into the cell membrane. The correct molecular weight of a drug depends on its application. However, most drugs generally comprise small molecules with a molecular weight of less than 500 *Da*. This is because drug molecules have a higher likelihood of passing through a cell's membrane and have a lower likelihood of being affected by biometabolic reactions. The term QED is a metric used to evaluate a molecule's overall drug-likeness, which is a geometric mean of logP, HBA, HBD, PSA, number of rotatable bonds (ROTB), number of aromatic rings (AROM), and number of structural alerts (ALERTS). A molecule with a high QED value is more likely to be a promising drug candidate. Finally, DRD2 refers to a drug's activity toward dopamine receptor D2. The dopaminergic neurotransmission is regulated by the G protein-coupled receptor dopamine receptor D2, which is mainly expressed in the brain.

In the experiment aimed at discovering protein docking materials, QVina2[45]—a tool to discover the minimum-energy docking conformation and calculate its docking score—was employed to compute a docking score. This score is proportional to the binding strength between a drug molecule and its target. QVina2 calculates the docking score by simulating how a drug

molecule interacts with a given target receptor in a three-dimensional simulation box. We targeted the protein receptor 5-HT<sub>1B</sub>. Many studies have reported that activating 5-HT<sub>1B</sub> receptors outside the brain has vascular effects (such as pulmonary vasoconstriction, which can help treat angina[52]). Moreover, reduced 5-HT<sub>1B</sub> heteroreceptor activity can increase impulsive behaviour, whereas reduced 5-HT<sub>1B</sub> autoreceptor activity can have an antidepressant-like effect[53, 54].

In the experiment aimed at discovering HIV inhibitors, we selected three HIV-related targets: C-C chemokine receptor 5 (CCR5), HIV integrase (INT), and HIV reverse transcriptase (RT). Here, CCR5 is the immune system-related protein, which is found on the surface of white blood cells. Along with C-X-C chemokine receptor 4, it is a key co-receptor for HIV entry[55]. The second target was INT, which is involved in viral replication and facilitates the viral cDNA’s insertion into the infected cells[1]. The final target was RT, which triggers the reverse transcription process. Moreover, it has significant ramifications that mutation and recombination form the genetic diversity of HIV, enabling the formation of viral variants that could evade host immune responses, rendering the virus resistant to medication treatments[56]. For each target in the experiment, we tried to maximize its pIC<sub>50</sub> value, which is a descriptor for the potency of a drug in inhibiting a biological activity. It is calculated as the negative logarithm of the IC<sub>50</sub> value, which is the amount of a drug that inhibits 50% of the biological activity. In other words, the drug’s potency increases as the IC<sub>50</sub> value decreases. In the realm of drug discovery, IC<sub>50</sub> is commonly utilized to compare the effectiveness of potential drug candidates.

## 4.2 Fragment set configuration

Two types of fragment sets were used in this study. One set contained 2,207 BRICS fragments that appeared more than 150 times in the training set[22] curated from the ChEMBL database[22] (release version 25). This fragment set was used for the three major experiments: the discovery of seven target-hitting molecules, protein docking materials, and HIV inhibitors. For the supplementary experiment aimed at discovering five target-hitting molecules (Supplementary Note 1), another fragment set containing 2,547 BRICS fragments that appeared more than 100 times in the training set of the MOSES database[33] was used. The detailed reasoning for using these fragment sets is described in Supplementary Note 2.

## 4.3 Action masking

For efficient learning, we applied action masking to our model (Fig. 2g). Based on the molecule in the current state, the list of actions that the agent can choose is limited by action masking. Since our model combines fragments according to BRICS fragment combination rules, the fragments that could not be connected to the molecule in the current state were masked. Thereby, more efficient learning was possible since the number of selectable actions in the current state

was reduced, which improved the performance of our model (Supplementary Fig. 3b).

#### 4.4 Target properties and calculation of molecular descriptors

In this study, three major experiments were conducted to generate molecules with extreme properties. In the first experiment, discovering molecules that could hit the multiple target properties was attempted. In the other experiments, discoveries of molecules that either maximized or minimized interesting properties were attempted. Accordingly, the interesting properties could be calculated by the evaluators in the environment of the RL model.

For the first experiment on materials extrapolation to hit multiple extreme target properties, seven molecular descriptors were set as the targets: logP[42], TPSA[43], QED[44], HBA, HBD, MW, and DRD2[22]. Here, the DRD2 was calculated using a QSAR model for DRD2[22], while the other descriptors were calculated using RDKit[41]. We selected 10 target sets of molecular properties out of known molecular data and attempted to generate the target-hitting molecules to demonstrate that our model would work well in terms of materials extrapolation. These 10 target sets of extreme properties were taken from an untrained dataset—PubChem SARS-CoV-2 clinical trials[47]—whose molecular properties are more widely distributed than the training data set[22] training (Fig. 3a). Since the ten target sets of extreme properties were taken from real molecules, they could be considered chemically feasible targets to discover.

For the experiment to discover protein docking materials, the calculated docking score between a docking molecule and HT<sub>1B</sub> protein receptor was set as the target. The docking score was calculated using QVina2[45], which calculates the docking score of a docking molecule by searching for its minimum-energy docking conformation. This program employs an empirical scoring function to predict the docking score, which includes a number of terms that incorporate various physical and chemical interactions between the ligand and protein. These interactions include van der Waals interactions, electrostatic interactions, hydrogen bonds, and solvation effects. Moreover, QVina2 makes use of finely tuned scoring function parameters that are derived using many experimentally-identified ligand-protein complexes. It calculates a docking score for each docking posture it produces, with the lowest value being the most energetically favourable binding conformation. The detailed calculation configuration for QVina2 is illustrated in Supplementary Note 4.

For the experiment to discover HIV inhibitors, the target property was set to maximize the pIC<sub>50</sub> score to three HIV-related targets: CCR5, INT, and RT. Each pIC<sub>50</sub> score was calculated by the light gradient boosting machine (LGBM)[57]-based QSAR models for the three HIV-related targets[4]. In addition, the QSAR model was trained to predict the pIC<sub>50</sub> value for each target using the ChEMBL dataset[34].

## 4.5 Training loop

To maximize the cumulative reward for sequential actions, RL trains its agent to learn which action to choose at each step. When the agent performs an action in the training process, the next state and reward are generated through the environment. In this study, the action was a selection of a molecular fragment and the next state was the molecule combined with the selected molecular fragment. The reward is the value calculated with the evaluator(s) by the experiment-specific reward function. By repeating this process, the policy that selects an action that can maximize the cumulative reward is gradually updated. After sufficient learning, the policy could then select sequential actions to generate a desired molecule that fits the given task.

The episode proceeds from steps 0 to  $T$ , where  $T$  is the designated maximum fragment number of the molecule. To produce diverse molecules, the first fragment is randomly selected. When selecting the next molecular fragment to be combined with the current molecule, action masking is conducted. In the process of action masking, the molecular fragments that cannot be combined with the current molecule are masked according to the BRICS fragmentation combination rules. Subsequently, the policy selects a molecular fragment from the unmasked fragments and binds it to an unfilled binding site. If the combined molecule still has any unfilled binding sites, hydrogen atoms are attached to derive a complete molecule and evaluate its properties of the current state. When a molecule that meets the set of criteria (or one of the termination conditions) is generated, the fragment attachment is stopped and the episode ends early before reaching step  $T$ . Otherwise, the process is repeated during step  $T$ . After the final output molecule is generated, a reward for the episode is calculated depending on how closely the targets are hit. By iteratively conducting the training episodes, the agent of RL learns a policy that maximizes the given reward function. The episode training is repeated until a preset number of training iterations is reached. For each experiment, the training iteration was set to 750, 80, and 250 times.

## 4.6 Rewards and terminations

In RL, it is important to have an appropriate set of termination conditions to learn a decent policy. In all three experiments conducted in this study, there were two common termination conditions. First, molecular generation was terminated when the number of fragments that make up a compound in the current state  $n_{eval}$  exceeded the maximum number of fragments ( $n_{max}$ ), which was set to 50, 4, and 6 for each experiment. Second, the process was terminated when the number of unfilled binding sites ( $n_L$ ) was equal to zero.

For the experiment on materials extrapolation to hit multiple extreme target properties, two more termination conditions were applied. First, the process was terminated if the  $MW$  in the current state ( $MW_{eval}$ ) exceeded the maximum  $MW$  ( $MW_{max} = 3500Da$ ). Second, the process was terminated if the

error ( $\epsilon$ ) was less than the error threshold  $\epsilon_{th} = 0.05$ . Here,  $\epsilon$  was calculated as

$$\epsilon = \sum_{y \in prop.} \left( \frac{y_{trg.} - y_{eval.}}{\sigma_y} \right)^2 \quad (7)$$

where  $y_{trg.}$ ,  $y_{eval.}$ , and  $\sigma_y$  denote the target  $y$ , evaluated  $y$ , and standard deviation of  $y$  for the curated ChEMBL training set[22], respectively. Here, *prop* is a set of properties that includes logP, TPSA, QED, HBA, HBD, MW, and DRD2.

The design of the reward function is also important since RL is performed based on the reward obtained by taking an action. Moreover, a penalty can be given to avoid any undesired actions. For the experiment on materials extrapolation to hit multiple extreme target properties, the reward function  $r$  was designed as follows:

$$r = \begin{cases} 0, & \text{if } \{[MW_{eval.} < MW_{min.}] \vee [n_{eval.} < n_{min.}]\} \wedge [n_L \neq 0], \\ -50, & \text{if } \{[MW_{eval.} < MW_{min.}] \vee [n_{eval.} < n_{min.}]\} \wedge [n_L = 0], \\ \frac{100}{\epsilon+1}, & \text{else if } \epsilon < \epsilon_{th.}, \\ \frac{30}{\epsilon+1}, & \text{otherwise.} \end{cases} \quad (8)$$

Here,  $MW_{min}$  and  $n_{min}$  were set to generate various compounds by avoiding premature termination, which would generate uniform molecules that were too small. For this purpose, when the number of unfilled binding sites  $n_L$  was not equal to zero, a zero reward was given if  $MW_{eval.}$  was less than  $MW_{min}$  or  $n_{eval.}$  was less than  $n_{min.}$  When  $n_L$  was equal to zero, a reward of  $-50$  was given if  $MW_{eval.}$  was less than  $MW_{min}$  or  $n_{eval.}$  was less than  $n_{min.}$  However, if it deviated from the above two cases, a reward proportional to the degree of proximity to the target was awarded.

For the other two experiments (discovery of protein docking materials and HIV inhibitors), the reward function  $r$  was designed as follows:

$$r = \begin{cases} 0, & \text{if } \{[MW_{eval.} < MW_{min.}] \vee [n_{eval.} < n_{min.}]\} \wedge [n_L \neq 0], \\ -50, & \text{if } \{[MW_{eval.} < MW_{min.}] \vee [n_{eval.} < n_{min.}]\} \wedge [n_L = 0], \\ \text{Predicted Score}, & \text{otherwise.} \end{cases} \quad (9)$$

Here, the predicted score refers to the calculated docking and pIC<sub>50</sub> scores of the HIV-related target, respectively.

## 4.7 RL algorithm

We performed benchmark testing against the following state-of-the-art RL algorithms: IMPALA[58], APPO[59], A2C & A3C[60], and PPO[46]. The detailed results of the benchmarking are summarized in Supplementary Note 3. From the benchmark results, we confirmed that PPO—which is a model-free, on-policy, actor-critic, and policy-gradient algorithm—was the most suitable

for our problems, with a very large discrete action space of over 2,000. Moreover, PPO is known for its good performance, stability, and good sample efficiency, which makes the training process more stable by avoiding large policy updates with importance sampling and reusing learning data on the trust region. Hence, we applied PPO for all experiments conducted in this study. The objective function of PPO is defined as follows:

$$L^{CLIP}(\theta) = \hat{E}[\min(r_t(\theta)\hat{A}_t, \text{clip}(r_t)(\theta), 1 - \epsilon, 1 + \epsilon)\hat{A}_t],$$

$$\text{where } r_t(\theta) = \frac{\pi_\theta(a_t | s_t)}{\pi_{\theta_{\text{old}}}(a_t | s_t)} \quad (10)$$

where  $\hat{E}_t$  represents the expected value at time step  $t$ . Term  $r_t$  denotes the ratio between the new policy  $\pi_\theta$  and the old policy  $\pi_{\theta_{\text{old}}}$ . The policy is expressed as  $\pi_\theta(a_t | s_t)$ , where  $a_t$  and  $s_t$  are the action and state at timestep  $t$ , respectively. In Equation 10,  $\hat{A}_t$  denotes the advantage function at time step  $t$ , which estimates the result of the step action more effectively than the behaviour of the default policy.

## 4.8 Further findings

We empirically demonstrated that our methodology can discover novel materials with extreme properties, which is impossible to accomplish with existing models that learn the probability distribution of data. However, there were two limitations with our model, which could be solved through further studies. First, the model should be re-trained if the target changes because the reward function depends on the given target. Therefore, the model must learn the policy from the start each time a new target is set. To solve this problem, a methodology such as meta-learning may be applied in future studies. With meta-learning, it is possible to predict the results of a new task or recommend hyperparameters based on the learning results from another task. Therefore, when a new task is assigned, it will be possible to learn through the experiences that have been taught in the past, requiring less additional training. For example, using methods such as MetaGenRL[61], which applies meta-learning to reinforcement learning, the model outperformed the existing reinforcement learning algorithm while exhibiting similar performance for completely different tasks. Second, there was a sparse reward problem, which occurred because the agent received little feedback or reward for the action from the environment, rendering it difficult to learn efficient policies and satisfy the desired goal. Since molecules with extreme properties are rarer than common molecules, the probability of experiencing an episode in which a rare molecule is obtained through a random combination of molecular fragments is relatively low. To solve this problem, we could adopt methods that encourage more exploration with curiosity. This would allow experiencing more episodes that could provide higher rewards. In addition, hierarchical reinforcement learning[62] could be applied, which is a methodology that utilizes prior knowledge of the

given problem to set sub-goals that are easier to achieve than the original goal. Accordingly, it learns a policy that can achieve the original goal through policies learned from sub-goals.

**Supplementary information.** Supplementary Information is available at url (TBA).

**Data availability.** The curated ChEMBL datasets and MOSES data sets for training and testing cRNN[22] and GCT[21] are publically available at <https://github.com/MolecularAI/Deep-Drug-Coder> and <https://github.com/molecularsets/moses>, respectively.

**Code availability.** The code for this study is available upon reasonable request to the corresponding authors.

**Competing interest.** The authors have no competing interests to declare.

**Author contributions.** H.K. proposed the concept of materials extrapolation and the scheme of AI-driven combinatorial chemistry. H.K., H.C., and J.N. designed the experiments, and they were implemented by H.K., H.C., and D.K. All authors analysed the results and discussed them. H.K., H.C., and D.K. wrote the manuscript, and all authors reviewed it. J.N. and W.B.L. supervised the project.

**Acknowledgments.** This research was supported by the National Research Foundation of Korea (NRF) grant funded by the Korean Government through the Ministry of Science and ICT (MSIT) (NRF-2021R1C1C1012031, NRF-2021R1A4A3025742, NRF-2020M3F7A1094299, and NRF-2018M3D1A1058633).

## References

- [1] Pommier, Y., Johnson, A.A., Marchand, C.: Integrase inhibitors to treat hiv/aids. *Nature reviews Drug discovery* **4**(3), 236–248 (2005)
- [2] Yang, S., Hwang, D., Lee, S., Ryu, S., Hwang, S.J.: Hit and lead discovery with explorative rl and fragment-based molecule generation. *Advances in Neural Information Processing Systems* **34**, 7924–7936 (2021)
- [3] Kitchen, D.B., Decornez, H., Furr, J.R., Bajorath, J.: Docking and scoring in virtual screening for drug discovery: methods and applications. *Nature reviews Drug discovery* **3**(11), 935–949 (2004)
- [4] Gottipati, S.K., Sattarov, B., Niu, S., Pathak, Y., Wei, H., Liu, S., Blackburn, S., Thomas, K., Coley, C., Tang, J., *et al.*: Learning to navigate the synthetically accessible chemical space using reinforcement learning. In: *International Conference on Machine Learning*, pp. 3668–3679 (2020). PMLR

- [5] Klein, A., Körber, C., Wachau, A., Säuberlich, F., Gassenbauer, Y., Harvey, S.P., Proffit, D.E., Mason, T.O.: Transparent conducting oxides for photovoltaics: Manipulation of fermi level, work function and energy band alignment. *Materials* **3**(11), 4892–4914 (2010)
- [6] Greenaway, R.L., Jelfs, K.E.: Integrating computational and experimental workflows for accelerated organic materials discovery. *Advanced Materials* **33**(11), 2004831 (2021)
- [7] Sylvinson MR, D., Chen, H.-F., Martin, L.M., Saris, P.J., Thompson, M.E.: Rapid multiscale computational screening for oled host materials. *ACS applied materials & interfaces* **11**(5), 5276–5288 (2019)
- [8] Kim, K., Kang, S., Yoo, J., Kwon, Y., Nam, Y., Lee, D., Kim, I., Choi, Y.-S., Jung, Y., Kim, S., *et al.*: Deep-learning-based inverse design model for intelligent discovery of organic molecules. *npj Computational Materials* **4**(1), 1–7 (2018)
- [9] Meredig, B., Antono, E., Church, C., Hutchinson, M., Ling, J., Paradiso, S., Blaiszik, B., Foster, I., Gibbons, B., Hattrick-Simpers, J., *et al.*: Can machine learning identify the next high-temperature superconductor? examining extrapolation performance for materials discovery. *Molecular Systems Design & Engineering* **3**(5), 819–825 (2018)
- [10] Ling, J., Hutchinson, M., Antono, E., Paradiso, S., Meredig, B.: High-dimensional materials and process optimization using data-driven experimental design with well-calibrated uncertainty estimates. *Integrating Materials and Manufacturing Innovation* **6**(3), 207–217 (2017)
- [11] Pyzer-Knapp, E.O., Suh, C., Gómez-Bombarelli, R., Aguilera-Iparraguirre, J., Aspuru-Guzik, A.: What is high-throughput virtual screening? a perspective from organic materials discovery. *Annual Review of Materials Research* **45**, 195–216 (2015)
- [12] Liu, J., Gong, S., Li, H., Liu, G.: Molecular graph-based deep learning method for predicting multiple physical properties of alternative fuel components. *Fuel* **313**, 122712 (2022)
- [13] Dan, Y., Zhao, Y., Li, X., Li, S., Hu, M., Hu, J.: Generative adversarial networks (gan) based efficient sampling of chemical composition space for inverse design of inorganic materials. *npj Computational Materials* **6**(1), 1–7 (2020)
- [14] SV, S.S., Law, J.N., Tripp, C.E., Duplyakin, D., Skordilis, E., Biagioni, D., Paton, R.S., St John, P.C.: Multi-objective goal-directed optimization of de novo stable organic radicals for aqueous redox flow batteries. *Nature Machine Intelligence*, 1–11 (2022)

- [15] Dong, Y., Li, D., Zhang, C., Wu, C., Wang, H., Xin, M., Cheng, J., Lin, J.: Inverse design of two-dimensional graphene/h-bn hybrids by a regressional and conditional gan. *Carbon* **169**, 9–16 (2020)
- [16] Lyu, M.-Y., Choi, T.G.: Research trends in polymer materials for use in lightweight vehicles. *International journal of precision engineering and manufacturing* **16**(1), 213–220 (2015)
- [17] Stauber, R.: Plastics in automotive engineering. *ATZ worldwide* **109**(3), 2–4 (2007)
- [18] Zunger, A.: Inverse design in search of materials with target functionalities. *Nature Reviews Chemistry* **2**(4), 1–16 (2018)
- [19] Méndez-Lucio, O., Baillif, B., Clevert, D.-A., Rouquié, D., Wichard, J.: De novo generation of hit-like molecules from gene expression signatures using artificial intelligence. *Nature communications* **11**(1), 1–10 (2020)
- [20] Lim, J., Ryu, S., Kim, J.W., Kim, W.Y.: Molecular generative model based on conditional variational autoencoder for de novo molecular design. *Journal of cheminformatics* **10**(1), 1–9 (2018)
- [21] Kim, H., Na, J., Lee, W.B.: Generative chemical transformer: Neural machine learning of molecular geometric structures from chemical language via attention. *Journal of Chemical Information and Modeling* **61**(12), 5804–5814 (2021)
- [22] Kotsias, P.-C., Arús-Pous, J., Chen, H., Engkvist, O., Tyrchan, C., Bjerrum, E.J.: Direct steering of de novo molecular generation with descriptor conditional recurrent neural networks. *Nature Machine Intelligence* **2**(5), 254–265 (2020)
- [23] Sutskever, I., Vinyals, O., Le, Q.V.: Sequence to sequence learning with neural networks. *Advances in neural information processing systems* **27** (2014)
- [24] Vaswani, A., Shazeer, N., Parmar, N., Uszkoreit, J., Jones, L., Gomez, A.N., Kaiser, L., Polosukhin, I.: Attention is all you need. *Advances in neural information processing systems* **30** (2017)
- [25] Mirza, M., Osindero, S.: Conditional generative adversarial nets. *arXiv preprint arXiv:1411.1784* (2014)
- [26] Sohn, K., Lee, H., Yan, X.: Learning structured output representation using deep conditional generative models. *Advances in neural information processing systems* **28** (2015)

- [27] Goodfellow, I., Pouget-Abadie, J., Mirza, M., Xu, B., Warde-Farley, D., Ozair, S., Courville, A., Bengio, Y.: Generative adversarial nets. *Advances in neural information processing systems* **27** (2014)
- [28] Kingma, D.P., Welling, M.: Auto-encoding variational bayes. *arXiv preprint arXiv:1312.6114* (2013)
- [29] Guimaraes, G.L., Sanchez-Lengeling, B., Outeiral, C., Farias, P.L.C., Aspuru-Guzik, A.: Objective-reinforced generative adversarial networks (organ) for sequence generation models. *arXiv preprint arXiv:1705.10843* (2017)
- [30] Sanchez-Lengeling, B., Outeiral, C., Guimaraes, G.L., Aspuru-Guzik, A.: Optimizing distributions over molecular space. an objective-reinforced generative adversarial network for inverse-design chemistry (organic) (2017)
- [31] Blaschke, T., Olivecrona, M., Engkvist, O., Bajorath, J., Chen, H.: Application of generative autoencoder in de novo molecular design. *Molecular informatics* **37**(1-2), 1700123 (2018)
- [32] Griffiths, R.-R., Hernández-Lobato, J.M.: Constrained bayesian optimization for automatic chemical design using variational autoencoders. *Chemical science* **11**(2), 577–586 (2020)
- [33] Polykovskiy, D., Zhebrak, A., Sanchez-Lengeling, B., Golovanov, S., Tatanov, O., Belyaev, S., Kurbanov, R., Artamonov, A., Aladinskiy, V., Veselov, M., *et al.*: Molecular sets (moses): a benchmarking platform for molecular generation models. *Frontiers in pharmacology* **11**, 1931 (2020)
- [34] Mendez, D., Gaulton, A., Bento, A.P., Chambers, J., De Veij, M., Félix, E., Magariños, M.P., Mosquera, J.F., Mutowo, P., Nowotka, M., *et al.*: ChEMBL: towards direct deposition of bioassay data. *Nucleic acids research* **47**(D1), 930–940 (2019)
- [35] Furka, A.: Study on the possibilities of systematic searching for pharmaceutically useful peptides. Notarized Report (File number 36237/1982, in Hungarian) (1982)
- [36] Degen, J., Wegscheid-Gerlach, C., Zaliani, A., Rarey, M.: On the art of compiling and using ‘drug-like’ chemical fragment spaces. *ChemMedChem: Chemistry Enabling Drug Discovery* **3**(10), 1503–1507 (2008)
- [37] Bohacek, R.S., McMartin, C., Guida, W.C.: The art and practice of structure-based drug design: a molecular modeling perspective. *Medicinal research reviews* **16**(1), 3–50 (1996)

- [38] Klaus, K.: Web dictionary of cybernetics and systems. Principia Cybernetica Web (1986)
- [39] Shannon, C.E.: A mathematical theory of communication. ACM SIGMOBILE mobile computing and communications review **5**(1), 3–55 (2001)
- [40] Kullback, S., Leibler, R.A.: On information and sufficiency. The annals of mathematical statistics **22**(1), 79–86 (1951)
- [41] RDKit: Open-source cheminformatics. <http://www.rdkit.org>. [Online; accessed 02-June-2022]
- [42] Wildman, S.A., Crippen, G.M.: Prediction of physicochemical parameters by atomic contributions. Journal of chemical information and computer sciences **39**(5), 868–873 (1999)
- [43] Ertl, P., Rohde, B., Selzer, P.: Fast calculation of molecular polar surface area as a sum of fragment-based contributions and its application to the prediction of drug transport properties. Journal of medicinal chemistry **43**(20), 3714–3717 (2000)
- [44] Bickerton, G.R., Paolini, G.V., Besnard, J., Muresan, S., Hopkins, A.L.: Quantifying the chemical beauty of drugs. Nature chemistry **4**(2), 90–98 (2012)
- [45] Alhossary, A., Handoko, S.D., Mu, Y., Kwoh, C.-K.: Fast, accurate, and reliable molecular docking with quickvina 2. Bioinformatics **31**(13), 2214–2216 (2015)
- [46] Schulman, J., Wolski, F., Dhariwal, P., Radford, A., Klimov, O.: Proximal policy optimization algorithms. arXiv preprint arXiv:1707.06347 (2017)
- [47] PubChem: PubChem SARS-Cov-2 Clinical Trials. <https://pubchem.ncbi.nlm.nih.gov/docs/covid-19> Accessed accessed: 05.06.2022
- [48] Zhang, H., Gong, X., Peng, Y., Saravanan, K.M., Bian, H., Zhang, J.Z., Wei, Y., Pan, Y., Yang, Y.: An efficient modern strategy to screen drug candidates targeting rdrp of sars-cov-2 with potentially high selectivity and specificity. Frontiers in chemistry **10** (2022)
- [49] Wang, Y., Xiao, J., Suzek, T.O., Zhang, J., Wang, J., Zhou, Z., Han, L., Karapetyan, K., Dracheva, S., Shoemaker, B.A., *et al.*: Pubchem’s bioassay database. Nucleic acids research **40**(D1), 400–412 (2012)
- [50] Hillhouse, E., Grammatopoulos, D.: Control of intracellular signalling by corticotropin-releasing hormone in human myometrium. Frontiers of

hormone research **27**, 66–74 (2001)

- [51] Kawasaki, H., Springett, G.M., Mochizuki, N., Toki, S., Nakaya, M., Matsuda, M., Housman, D.E., Graybiel, A.M.: A family of camp-binding proteins that directly activate rap1. *Science* **282**(5397), 2275–2279 (1998)
- [52] Morecroft, I., Heeley, R.P., Prentice, H.M., Kirk, A., MacLean, M.R.: 5-hydroxytryptamine receptors mediating contraction in human small muscular pulmonary arteries: importance of the 5-ht1b receptor. *British journal of pharmacology* **128**(3), 730–734 (1999)
- [53] Nautiyal, K.M., Tanaka, K.F., Barr, M.M., Tritschler, L., Le Dantec, Y., David, D.J., Gardier, A.M., Blanco, C., Hen, R., Ahmari, S.E.: Distinct circuits underlie the effects of 5-ht1b receptors on aggression and impulsivity. *Neuron* **86**(3), 813–826 (2015)
- [54] Clark, M., Neumaier, J.: The 5-ht1b receptor: behavioral implications. *Psychopharmacology bulletin* **35**(4), 170–185 (2001)
- [55] Huang, Y., Paxton, W.A., Wolinsky, S.M., Neumann, A.U., Zhang, L., He, T., Kang, S., Ceradini, D., Jin, Z., Yazdanbakhsh, K., *et al.*: The role of a mutant ccr5 allele in hiv-1 transmission and disease progression. *Nature medicine* **2**(11), 1240–1243 (1996)
- [56] Sarafianos, S.G., Marchand, B., Das, K., Himmel, D.M., Parniak, M.A., Hughes, S.H., Arnold, E.: Structure and function of hiv-1 reverse transcriptase: molecular mechanisms of polymerization and inhibition. *Journal of molecular biology* **385**(3), 693–713 (2009)
- [57] Ke, G., Meng, Q., Finley, T., Wang, T., Chen, W., Ma, W., Ye, Q., Liu, T.-Y.: Lightgbm: A highly efficient gradient boosting decision tree. *Advances in neural information processing systems* **30** (2017)
- [58] Espeholt, L., Soyer, H., Munos, R., Simonyan, K., Mnih, V., Ward, T., Doron, Y., Firoiu, V., Harley, T., Dunning, I., *et al.*: Impala: Scalable distributed deep-rl with importance weighted actor-learner architectures. In: *International Conference on Machine Learning*, pp. 1407–1416 (2018). PMLR
- [59] Schulman, J., Wolski, F., Dhariwal, P., Radford, A., Klimov, O.: Proximal policy optimization algorithms. *arXiv preprint arXiv:1707.06347* (2017)
- [60] Mnih, V., Badia, A.P., Mirza, M., Graves, A., Lillicrap, T., Harley, T., Silver, D., Kavukcuoglu, K.: Asynchronous methods for deep reinforcement learning. In: *International Conference on Machine Learning*, pp. 1928–1937 (2016). PMLR

- [61] Kirsch, L., van Steenkiste, S., Schmidhuber, J.: Improving generalization in meta reinforcement learning using learned objectives. arXiv preprint arXiv:1910.04098 (2019)
- [62] Riedmiller, M., Hafner, R., Lampe, T., Neunert, M., Degraeve, J., Wiele, T., Mnih, V., Heess, N., Springenberg, J.T.: Learning by playing solving sparse reward tasks from scratch. In: International Conference on Machine Learning, pp. 4344–4353 (2018). PMLR